NASA TECHNICAL MEMORANDUM

NASA TM X-67894

NASA TM X-67894

BERYLLIUM BEHAVIOR IN THE NASA PLUM BROOK REACTOR

by R. A. Hasse
Lewis Research Center
Cleveland, Ohio

TECHNICAL PAPER proposed for presentation at Fifth Conference of the Reactor Operations Division of the American Nuclear Society
Denver, Colorado, August 9-11, 1971

ABSTRACT

Two beryllium structural plates in the NASA Plum Brook Reactor have bowed toward the fuel core, and eventually failed by gross cracking. This behavior was evaluated in terms of mechanical and physical property changes of the irradiated material, internal and external stresses experienced by the plates, plate fabrication techniques, and reactor operating history. The preliminary evaluation did not permit firm conclusions to be drawn. However, the amount of bow per unit dose was proportional to the mean reactor power level. The internal stresses alone may have approached the measured tensile strength of the beryllium.

E-6499

BERYLLIUM BEHAVIOR IN THE NASA PLUM BROOK REACTOR

by R. A. Hasse

Lewis Research Center

E-6499

SUMMARY

The NASA Plum Brook Reactor (PBR) has suffered structural failure of 2 beryllium reflector plates in 8 years of operation. A preliminary evaluation of the failures has been performed in terms of mechanical property changes, internal and external stresses on the plates, fabrication methods, microstructure, and reactor operating history.

Mechanical property changes were determined by tensile and bend tests on surveillance material. Internal stresses were determined by analyzing the plate material for changes in density and lattice parameters, linear growth, and gas content. The external stress is exerted as a hydraulic force on the plates, which act as flow dividers.

Data scatter prevented the precise determination of the increases in tensile and bend strengths. The increases appeared to be in the range of 25-50 percent at fluences up to 9×10^{21} n/cm^2 ($E_n > 0.1$ Mev). Transmission electron microscopy showed a dislocation loop density for the plate material of $\sim 5 \times 10^{15}$/cm^3 at a fluence of 2.4×10^{22} n/cm^2 ($E_n > 0.1$ Mev). The helium content for the same material was 11 cm^3/gm. The beryllium density decreased ~ 0.6 percent and the lattice parameters increased 0.05 and 0.09 percent for A_0 and C_0, respectively. The data indicated that the amount of plate bow per unit dose is directly proportional to the mean reactor power level and the total dose at failure is inversely proportional to the mean power level over the life of the plate.

It is shown that the internal stresses in the plates probably approach the tensile strength of the material and minimal external forces are required for plate failure. The effect of fabrication technique on the life of these plates is felt to be minimal.

INTRODUCTION

The NASA Plum Brook Reactor (PBR) has suffered structural failure of 2 beryllium reflector plates in its first 8 years of operation.

The replacement of failed reflector plate represents a significant cost consisting of reactor down time as well as the procurement cost of the plates. By evaluating the past failures, we hoped to identify the contributing factors to these failures and whether they could be easily eliminated or minimized.

This paper presents preliminary evaluation of these failures in terms of the observed microstructural, chemical, and mechanical property changes of beryllium in the PBR, the stresses experienced by the plates, and the operating history of the reactor. A brief description of the radiation damage mechanisms in beryllium will be presented first. The materials and their environment will then be described along with the observed material behavior. An analysis of the plate material consisting of density, lattice parameters, gas content, and microstructure will be presented followed by a summary of mechanical property changes. Finally, the material behavior will be evaluated in terms of the property changes, the stresses experienced by the plates, and reactor operating history.

SYMBOLS

B	bow of reflector plate, defined as maximum distortion from original plane of the plate
B_d	bow per unit equivalent dose
D	dose
D_e	equivalent dose used to compare north reflector plates to south reflector plates
D_f	dose at failure of reflector plate
E_n	energy of neutron
E	modulus of elasticity
K_b	bowing constant = $B_d/\overline{P}_r$
K_f	failure constant = $D_f \times \overline{P}_r$
n	neutron
N1,N2,...	first north reflector plate, second north reflector plate, ...
$\overline{P}_r$	mean power level of the reactor
S	stress
S1,S2,...	first south reflector plate, second south reflector plate, ...
ε	linear strain
μ	Poisson's ratio

RADIATION DAMAGE MECHANISMS IN BERYLLIUM

Beryllium suffers two types of damage under neutron irradiation. The first results from the displacement of lattice atoms struck by the incident neutrons. The second results from nuclear reactions between the Be atoms and the incident neutrons forming gaseous reaction products. Although these processes and their products are distinct, their ultimate effects on the material are similar. Both result in loss of material toughness, material growth, and high internal stresses.

The extent and type of damage occurring for a given neutron fluence is dependent on the irradiation temperature. The discussion below will be restricted primarily to damage occurring at the PBR ambient temperature of 340 K.

Formation of Deflected Structure

Formation of point defects, clusters, and dislocations. - A neutron passing through the beryllium material will displace lattice atoms leaving interstitial beryllium atoms and vacancies (point defects) in its wake. Some defect clusters, multiple vacancies and interstitials, may also be formed. The displaced beryllium atoms may be displaced with sufficient energy to cause similar damage themselves. To cause any damage of this type, the incident neutron must have enough energy to permanently displace at least one beryllium atom, ~ 25 eV (Ref. 1). The total amount of damage caused by a single neutron depends, of course, on its initial energy.

The point defects are mobile. As the point defects migrate, several things happen: vacancies and interstitials annihilate each other; multiple vacancies or interstitials (clusters) are formed; and some point defects are trapped by impurity atoms or annihilated at grain boundaries.

The clusters formed by the migration of point defects and the primary event may then collapse into dislocation loops. It is these clusters and loops that drastically affect the plastic properties of irradiated material.

Formation and behavior of gaseous atoms. - The second type of damage suffered by beryllium in a neutron flux is the formation of gaseous atoms. Although four different gases are formed, about 90 percent is helium-4. These atoms are formed by the following nuclear reactions:

$$Be^9 + N_f \rightarrow Be^8 + 2\ n \qquad (1)$$

$$Be^8 \rightarrow 2\ He^4 \qquad (2)$$

$$Be^9 + N_f \rightarrow He^6 + He^4 \qquad (3)$$

$$He^6 \xrightarrow{\beta^-} Li^6 \qquad (4)$$

$$Li^6 + N_t \quad H^3 + He^4 \tag{5}$$

$$H^3 \xrightarrow{\beta^-} He^3 \tag{6}$$

$$He^3 + N_t \rightarrow H^3 + H \tag{7}$$

The helium formed will occupy either interstitial positions in the beryllium lattice or to a lesser extent voids in the lattice. The presence of a helium atom in a void decreases the probability of a beryllium interstitial being annihilated by a vacancy and thus increases the probability of cluster formation.

As the temperature and gas concentration increase, gas bubbles can from. These bubbles are probably nucleated by vacancies and vacancy clusters. However, at the temperature and gas concentration of concern here, the formation of bubbles has not been observed.

Effects of Defected Structure

The defected structure consists of point defects, vacancy and interstitial clusters, dislocations, interstitial gas atoms and gas atoms occupying lattice vacancies. The effect of these defects on the properties of beryllium are discussed briefly below.

Material growth. - Both types of radiation damage, gas formation and atom displacement, contribute to the growth of beryllium in a neutron flux. An interstitial Be atom will occupy a volume approaching that of a lattice site. The collapse of the lattice about the vacancy left by the Be atom is relatively small. For a typical metal, Thompson (Ref. 1) has estimated that the collapse about a spherical void with a radius of one Å is ~ 0.1 Å. More importantly, he has shown that the absolute value of this collapse is dependent only on the shear modulus of elasticity and the surface energy of the metal and independent of the void radius. Thus, as void or vacancy clusters grow, collapse becomes less important, remaining at ~ 0.1 Å on the radius for the typical metal.

The same arguments given above can be applied to interstitial and vacancy dislocation loops. Thus, these dislocations also cause material growth.

When beryllium is transmuted by a neutron, at least 2 gas atoms are formed. This was shown in the nuclear reactions given earlier. Although the bulk of the gas is helium with a small atomic radius, there is still a net increase in volume. The net increase in volume will depend on the fraction of gas atoms occupying the vacancies, interstitial positions, voids and other trapping sites.

Internal stresses. - There are obviously internal stresses present in the defected structure. These result from the collapse of the lattice

about vacancies, vacancy loops and clusters and stretching around interstitials, interstitial loops and clusters. They also result from the dilation of the lattice by the gas atoms. The stresses are related to the material growth by the elastic modulus.

Elastic properties. - No experimental work on the elastic properties of irradiated beryllium has been reported. Some work has been done on copper (Ref. 2) which verifies theory. Initially, the formation of point defects which pin dislocations causes a rapid increase in Young's modulus. However, the magnitude of the increase is small and the effect saturates rapidly. Roth and Haundorf (Ref. 2) report that this increase is followed by a decrease in modulus for copper which they ascribe to a bulk effect; i.e., point defects changing the interatomic force constants. Although the changes again are small, there was no indication of saturation of this effect. The overall changes are probably restricted to several percent.

Plastic flow. - The mechanisms by which the defected structure changes the properties of a material are not completely understood. However, the change in elastic properties is generally ascribed to point defects since this involves only small movements (several angstroms) of the dislocations. In contrast, plastic flow requires large movements of the dislocations. In this case, clusters and dislocation interactions are felt to be the primary cause of property changes.

The ductility of beryllium decreases during irradiation. The amount depends on the type of material irradiated and the testing temperature. A compilation of data is given in Ref. 3. For hot pressed material at the temperatures of concern here, the ductility becomes effectively zero above a fluence of 10^{21} n/cm^2 (E_n > 1.0 Mev).

MATERIALS AND BEHAVIOR

The PBR core is a 9x3 array of aluminum clad MTR type fuel elements (Fig. 1). Thermal output is 60 megawatts. Removable beryllium reflector pieces surround the fueled core on the north, east, and west sides. Five control rods with beryllium followers are in alternate positions with the north removable reflector pieces. Four rows of eight beryllium pieces abut the south side of the fueled core and are separated from the core by a 2.54 centimeter thick 91 centimeter by 104 centimeter beryllium plate (south plate). A similar plate (north plate) forms the north side of the core box, outside the removable beryllium pieces. The cooling water flows up through the reflector on the first pass. Then it flows down through the fuel. The beryllium plates serve as barriers for the primary cooling water (PCW) flow. The plates have 0.635 centimeter diameter vertical holes on 1.27 centimeter centers bored completely through them to provide additional cooling.

Three north plates and 3 south plates have been used in the reactor to date. All have bowed toward the core. The first 2 south plates failed after different periods of operation. The third north and south plates are now in use.

Material Pedigree

The first north and south plates were fabricated from Brush Beryllium hot-pressed block. The second and third plates were fabricated from Berylco HP-12 not pressed block under the same basic specifications as the first plates. The second south plate was atypical in that it was rolled from 4.45 centimeters to 3.18 centimeters in thickness at 1090 K. The plate was then annealed at 1090 K and machined to final size.

Table I gives a typical analysis from the manufacturer's quality control report for the second and third plate material. No similar data are available for the first plates.

Environment

The significant environmental parameters for the failed plates are given in Table II. A detailed neutron spectrum is given in the appendix. The neutron fluxes on the two plates are nominally unchanged from one plate to another. However, the rate of dose accumulation averaged over the life of the plates is greater for the second and still greater for the third plate. This is due to different reactor operating history during the life of the plates.

As mentioned before, the plates act as flow dividers in the reactor core. Flow of the PCW is up through the reflector section and down through the core. This results in an approximate 2.76×10^5 N/m^2 load at the bottom of the plate applied in the direction of the core. This load decreases to essentially zero at the top of the plate.

The first plates were bolted in channels at the bottom and sides. Subsequent plates were bolted at the sides only. The top of the plates rest against the side of the core grid (Fig. 1). (During a large portion of the operating time of the second south plate, a different core grid was used which allowed a 0.05 centimeter gap between the top of the south plate and the grid prior to any plate bowing.) The first plates fit in the channels with minimal tolerances. The second and third plates were cut back 0.065 centimeters on each side and the bottom and reduced 0.0125 centimeters in thickness within the channels to allow for material growth.

Material Behavior

All beryllium in the PBR has bowed toward the higher flux regions. An earlier review and corrective actions necessary were presented by Fecych (Ref. 4). Only the north and south plates will be discussed here.

Table III summarizes the bowing and failure data for the 3 north and 3 south plates. The first south plate (S1) failed after 37,256 megawatt days of operation and the second south plate (S2) failed after 23,223 megawatt days (Fig. 2). One megawatt day is equivalent to 6.5×10^{17} n/cm^2 ($E_n > 0.1$ Mev) peak fluence on the south plates and 1.3×10^{17} n/cm^2 peak fluence on the north plates.

It is interesting to note that the bow per unit dose B_d is different even for identical materials and fabrication (N2 and N3). Further, B_d appears to be larger at the lower doses (compare the two sets of measurements for N3 and S3).

ANALYSIS OF FAILED PLATES

After the failed plates were removed from the reactor, they were taken to the PBR Hot Laboratory for examination. The width of the first plate, S1, was measured as a function of the distance from the top of the plate. The width at the core horizontal centerline was 0.10 centimeters greater than at the top of the plate. This corresponds to a 0.11 percent linear strain. The width of the second plate, S2, was not measured since fractures were present in the vertical planes.

The plates had an adherent gray coating on their surfaces. From x-ray diffraction and emission spectrographic analyses, it was determined to be an aluminum oxide containing a small percentage of beryllium oxide.

Samples of the plate material were taken for more detailed examination. The sample locations are shown in Fig. 2. The samples were removed with diamond tip core drills, using water as a coolant. The specimens were examined for density, swelling threshold, lattice parameters, gas content, and microstructure.

Test Descriptions

The samples were etched with a HNO_3-HF mixture prior to testing to remove the oxide layer from the ends. All testing was performed at the PBR except for the transmission electron microscopy.

Density and swelling threshold. - Density determinations were made by the immersion method. Weights were determined in air and carbon tetrachloride with an analytical balance. The wet measurements were performed in a secondary enclosure to minimize temperature variations of the

bath. The bath temperature was determined with a thermocouple calibrated against a standard mercury thermometer.

The swelling threshold was determined by annealing specimens for 24 hours at various temperatures in argon and redetermining their density. This was done for plate S1 material only.

Lattice parameters. - Lattice parameters were measured using standard X-ray techniques with a back reflection camera. The lines on the film were scanned with a double beam scanning microdensitometer to correct for any density variations across the width of the line. All density distributions were guassian and corrections were not necessary. The lines used were:

Angle	Plane	Radiation
70.7	104	$K\alpha_2$
70.9	104	$K\alpha_1$
72.0	121	$K\beta_1$
80.6	114	$K\beta_1$

The method described on page 511 of Mirkin (Ref. 5) was used to calculate A_0 and C_0. The final values of A_0 and C_0 were determined to ± 0.00025 Å and ± 0.0001 Å, respectively.

Gas content. - The helium and tritium content of the material was determined by heating and/or melting samples in a vacuum and measuring the gases evolved with a gas chromatograph system. Contamination prevented the determination of hydrogen content.

Most samples were heated to 1473 K, cooled, reheated to 1473 K, cooled, and then melted at 1773 K. Gases evolved during each cycle were measured. All of the tritium was evolved during the first heating cycle. About 90 percent of the helium was evolved during the two heating cycles. Several samples were melted directly. There was no data offset apparent between the two methods.

Microstructure. - Samples of both irradiated materials were examined by standard metallographic techniques and transmission electron microscopy (TEM).

The metallographic samples were mechanically polished and then etched with a 9/1 mixture of ethanol/hydrofluoric acid. The TEM examinations were performed and evaluated by S. H. Gelles of Battelle Memorial Institute.

Results And Discussion

The results of the testing on the plate material are given in Table IV. Dosimetry details are given in the appendix.

Density and lattice parameters. - The changes in density and lattice parameters must be determined by comparing the data for specimens of low fluence to those of high fluence. This is necessary since no control material is available for plate S1 and the control material available for plate S2 has been machined into mechanical test specimens. The added fabrication history could alter these properties.

The data present a consistent picture of material growth accompanied by an increase in lattice strain. The material from plate S2 appears to have a lesser change in these properties per unit fluence than plate S1. This could be due at least in part to the uncertainties in the fluences and data.

The swelling threshold for plate S1 material is shown in Fig. 3. The threshold occurrs at about 730 K and breakaway swelling at about 930 K.

Gas content. - The helium content per unit fast fluence for plate S1 is quite consistent at about $4.4\text{-}4.8 \times 10^{-22}$ cm^3/gram. This agrees well with data reported in Ref. 3. The data for plate S2 is not as consistent within itself at $2.3\text{-}4.1 \times 10^{-22}$ cm^3/gram per unit fluence and does not agree well with the data from plate S1. This is probably due to the flattening of the horizontal fast flux profile across the core (see appendix). No correction for this was made when estimating the fluences for plate S2. But, the production rate in plate S2 certainly did not exceed that in plate S1.

The tritium to helium ratios, though somewhat scattered, are reasonably consistent for both plates and agree with those reported in Ref. 3.

Microstructure. - Typical photomicrographs of irradiated plate material are shown in Fig. 4. The range of grain sizes appear to be about the same for the two materials. However, the proportion of smaller grains appears somewhat higher for the material from plate S2.

The transmission electron micrographs (Figs. 5 and 6) show an increasingly defected structure with increasing fluence. The dislocation loop densities given in Table IV are very approximate since the density varies considerably within a small area. The complexity of the dislocation structure is shown in Fig. 7. Figure 7(a) shows examples of helixes, bowed and jogged dislocations and dislocations pinned by loops. Figure 7(b) shows in more detail the interactions between dislocations and loops and pinning of larger loops by small ones.

ANALYSIS OF SURVEILLANCE SPECIMENS

A surveillance program has been maintined for the beryllium used in the PBR. Unfortunately, no test facilities are available in the reactor that have fluxes equal to or greater than that experienced by the south B_e plate. Thus, the surveillance data is after the fact. The data does, however, help in the evaluation of the behavior of B_e in the reactor.

The surveillance program consists of irradiating tensile and bend (rod) specimens of the subject material to various fluences and measuring the post-irradiation properties. The properties measured are ultimate tensile strength, load at fracture for bend specimens, density and hardness.

Test Description

The specimens are irradiated in the PBR in contact with the primary cooling water. Nominal specimen centerline temperature during irradiation is 335-355 K.

Each test consists of 3 tensile and 3 bend specimens. A group of control tensile and bend specimens are tested to obtain average pre-irradiation data. Several controls are then run with each post-irradiation test to assure there are no data offsets between tests.

Specimens for tests 2-4 (Table V) of plate S1 were tested as removed from the reactor. The specimens had an adherent deposit of aluminum and beryllium oxides on them. Prior to testing specimens for tests 5 and x for plate S1 and tests 1 and 2 for plate S2, the specimens were etched with a HNO_3-HF mixture to remove these deposits.

Tensile and bend tests. - The tensile and bend tests were run on a 4500 kilogram test machine. The crosshead speed for the tensile tests was 0.5 centimeter per minute. The bend test consisted of 3 point loading. The test was run with a crosshead speed of 0.05 centimeters per minute.

Density and hardness. - The density and hardness were determined for each tensile specimen before and after irradiation. Densities were determined by the immersion method using carbon tetrachloride. Two independent density determinations were made in each case. Three indentations were made for each hardness determination. Post irradiation measurements were made on unetched specimens for tests 2-4 of plate S1 and on etched specimens for the remainder.

Results

The results of the surveillance testing are given in Table V. Dosimetry details are given in the appendix.

Post irradiation mechanical test results are given as maximum and minimum values obtained. This is necessary because of the data scatter. The uncertainties shown for the density changes is the estimated standard deviation. This was obtained by conservatively assuming a standard deviation of ± 0.5 milligram for the weight determinations and $\pm 1^{\circ}$ K for determining the temperature of the liquid. The duplicate density determinations seldom differed by more than one Kg/m^3 and never more than 2 Kg/m^3.

Discussion

Of primary significance is the scatter in the mechanical test results for the irradiated specimens. Primary factors leading to scatter of this type are material integrity of the individual specimens, specimen condition, and for the tensile tests, axiality of loading. Material integrity is defined as the internal condition of the material; i.e., lack of flaws resulting from fabrication. Specimen condition is defined as surface integrity; i.e., the presence or lack of microcracks or notches. Axiality of loading is defined as the uniformity of the stress distribution over the specimen cross section normal to the plane of loading. Refs. 6 through 8 discuss the effect of these factors on the measured properties of brittle materials.

Extra care was taken with the tensile testing of tests 5 and X for plate S1 and tests 1 and 2 for plate S2. Specimens were carefully examined after ecthing to assure no visible surface flaws were present. The axiality of tensile loading was also checked. This was done by placing 4 strain gages at 90° intervals around the gage section of a 17-7 PH stainless steel tensile specimen of the same design as the plate S1 specimens. The specimen was then pulled in tension and the strain at each of the 4 points were compared. Variation was less than 3 percent which is within the recommendations of Ref. 9.

Multiple failures were frequent. The failure mode was both intergranular and transgranular.

There was a distinct decrease in density observed for specimens in test 5 and test X for plate S1. The decrease for test X seems somewhat large compared to test 5. However, considering the uncertainty in fluences and density changes, they are not completely out of line.

The results of the surveillance testing may be summarized briefly as follows:

1. A decrease in density is observed at fluences in excess of 5×10^{21} n/cm^2 ($E_n > 0.1$ Mev).

2. The true tensile strength of the material increases with irradiation to levels in excess of 4.4×10^8 N/m^2. However, the material becomes

so sensitive to localized stress concentrations that the practical or usable ultimate tensile strength may decrease to levels as low as 1.2×10^8 N/m^2.

3. The S1 and S2 material do not show significant differences in response to irradiation.

EVALUATION OF RESULTS

A preliminary evaluation of results will be conducted under three topics; material properties, material state, and parametric analysis. A more thorough analysis is currently being performed. The material properties will be inferred from the surveillance testing data. The material state will be assessed from the analyses on the plate material and operating stresses. The parametric analysis will evaluate the plate bowing and failures in terms of the two parameters, plate fabrication, and reactor operating history.

Material properties. - One may infer from Table V that the tensile and bend strengths do increase with irradiation. However, one may further infer that the practical or usable strength for externally applied stresses of the material will decrease. This decrease in practical strength is a result of extreme embrittlement causing increased notch and impact sensitivity (Ref. 10).

The apparent reduction in tensile strength in test X may not be due entirely to testing parameters and specimen condition. Although no gas bubbles were observed in the irradiated plate material, it is possible that very small bubbles may be nucleating in the grain boundaries (Ref. 10). This would result in the weakening of these grain boundaries.

There is one other potential grain boundary weakening mechanism for the plate material. The adherent oxide coating could react metallurgically with the base material weaking the grain boundaries at the surface. Since the stresses will be maximum on the convex side of the bowed plate, cracks could be initiated at these weakened locations. Since the material has no mechanism for relieving the stress concentrations, the cracks would propagate rapidly causing plate fracture.

In summary, the material has become extremely embrittled and sensitive to stress concentrations. Further, two potential mechanisms exist for grain boundary weakening, presenting sites for crack initiation.

Material state. - It is apparent from the information presented previously that the plates are in a state of considerable internal stress. The internal stresses result from the gas and dislocation formation in the plate. An external force is also present due to the pressure drop of the PCW as it flows around the plate.

The internal strain caused by the gas in the beryllium matrix may be estimated by using an atom radius of one angstrom and assuming they occupy predominantly interstitial positions in the beryllium lattice. This is reasonably conservative since it ignores bond effects and atom repulsion. Using the data for plate S1, the atomic volume of helium per cubic centimeter of beryllium is 2.2×10^{-3} cubic centimeters. This corresponds to a linear strain of 0.07 percent.

S. H. Gelles of Battelle Memorial Institute has estimated the linear strain due to the dislocations at about 0.03 percent. Thus, the total calculated strain is about 0.1 percent. This compares quite well with the measured growth in width of plate number 1 of 0.11 percent. The density decrease indicates a linear strain of 0.2 percent and the lattice parameters a strain of 0.05 and 0.09 percent for A_0 and C_0, respectively.

Knowing the internal strain, the internal stresses may be calculated. Since these stresses are triaxial, the following formula must be used (Ref. 11):

$$S = \frac{E[2\varepsilon\mu + (1 - \mu)\varepsilon]}{(1 + \mu)(1 - 2\mu)} \qquad (8)$$

where:

S = stress

E = modulus of elasticity = 2.78×10^{11} N/m^2

ε = linear strain, assumed equal in all directions

μ = Poisson's ratio = 0.20, assumed equal in all directions

Using a nominal linear strain of 0.1 percent, the internal stress along a given axis is calculated to be 4.6×10^8 N/m^2.

To compare this value to the measured tensile strength of the surveillance material, one must first correct the surveillance data to include the internal stresses. Since the internal stress is proportional to the fluence, the internal stress for specimens of test 5 is

$$\frac{4.8 \times 10^{21}}{2.4 \times 10^{22}} \times 4.6 \times 10^8 = 9.0 \times 10^7 \text{ N/m}^2$$

Adding this value to the maximum externally applied stress to failure, one obtains a corrected tensile strength of

$$4.4 \times 10^8 + 0.9 \times 10^8 = 5.3 \times 10 \text{ N/m}^2$$

which does not greatly exceed the internal stress of 4.6×10^8 N/m^2 of S1.

Thus, external stresses required for failure are relatively small.

Attempts to calculate the tensile stresses in the plate due to the hydraulic load have been frustrated by the large number of unknowns. However, the maximum tensile stresses on the core face of the plate have been estimated at $\sim 1.4 \times 10^8$ N/m^2. This is also the location of maximum internal stress.

One may summarize by stating that the internal stresses in the plate approach the measured tensile strength of the material and the external forces required to initiate failure, are small.

Parametric analysis. - There remains one significant item to be evaluated. The plates bowed at different rates per unit fluence and failures occurred at significantly different total fluences. This leads one to a parametric analysis. There are only two distinct parameters which may be evaluated: mean reactor power level and plate materials and fabrication. Plate materials and fabrication will be evaluated first.

Materials and fabrication: As mentioned earlier, the materials for all the plates were purchased under the same basic specifications. And except for plate S2, all plates were fabricated in the same manner. One would expect then, that there would be minimal mechanical property differences between the plates. The testing of control surveillance material supports this assumption. The bend and tensile strengths are essentially the same.

As stated earlier, plate S2 was rolled to approximately 30 percent reduction in thickness. This results in a slightly preferred orientation of the beryllium crystals in the plate. Since the properties of beryllium are non-isotropic this will affect the directional properties of the material. Gelles and Rudnich (Ref. 13) have studied the effect of preferred orientation on the biaxial properties of beryllium. Their conclusions based on the limited information available were that for optimum strength and ductility under biaxial stress conditions, a fine grain size material of intermediate texture be chosen. Texture here means degree of preferred orientation. Based on this information, plate S2 should have had more desirable properties for biaxial stress conditions. The material did appear to have a higher percentage of smaller grains and did have a moderately preferred texture, if any.

However, the improvement of properties on two axis is done at the expense of the properties on the third axis. The effect on plate behavior would then depend on the axial distribution of the applied stresses. As mentioned before, attempts to do this have been unsuccessful.

Actually, there is no indication that any significant property changes resulted from the rolling process. Table I shows that there was no ductility increase in the rolling direction. Thus, the amount of

preferred orientation must be very small. The strengthening in the rolling direction indicated in Table I was not confirmed by PBR testing of the surveillance material taken from the plate. The tensile and bend strengths determined at the PBR were the same for plates S2 and S3.

In summary, mechanical property differences between the plates, if any, were quite small.

Mean power level: The reactor power level during operation does not vary significantly. However, due to increasing plant efficiency, the percent operating time over the life of the plates increased continuously. This increased the mean power level, $(\overline{P}_r)$, over an extended time period. An attempt will be made to correlate the data from Table III using the mean power level.

The mean power level $(\overline{P}_r)$ will be defined as the total energy output of the reactor for the interval of the measurement divided by the calendar time over which it was accumulated. Bow per unit dose (B_d) is defined as the maximum distortion from the original plane of the plate divided by the equivalent accumulated dose (see note b for Table III). The following relationship will be tested:

$$B_d = K_b \overline{P}_r \qquad (9)$$

where K_b is defined as the bowing constant. Table VI gives the results of this evaluation.

An examination of Table VI shows the following:

1. The data for S1, S2 and the second measurement for S3 indicates that for higher doses, B_d is proportional to $\overline{P}_r$ regardless of total dose.

2. The data for N2 and the first measurement for S3 indicate that for a given though lower dose, B_d is proportional to $\overline{P}_r$.

3. The value of K_b decreases to a constant value as the total dose increases (see Fig. 8).

In summary, these limited data indicate that B_d is a function of $\overline{P}_r$ and, at lower doses, of total dose.

The initial rapid strain rate may be plastic strain resulting from the hydraulic forces and increasing internal stresses. The fact that the strain rate for a given $\overline{P}_r$ appears to approach a constant in the vicinity of 5000 MWD would support this hypothesis. A dose of 5000 MWD is equivalent to a fast fluence of about 3×10^{21} n/cm^2 ($E_n > 0.1$ Mev). And it is in this vicinity that beryllium loses any ability to deform plastically.

The reason for the mean power level dependency is not clear. It is perhaps the result of a stress relaxation mechanism related to microcreep (Ref. 12).

There is one other interesting observation one may make concerning the failed south plates. If one examines the relationship between the dose at failure (D_f) and the $\overline{P}_r$ over the life of the plate, one finds D_f inversely proportional to $\overline{P}_r$. That is, if

$$D_f = \frac{K_f}{\overline{P}_r} \tag{10}$$

where K_f is a failure constant, one obtains a K_f for plate S1 of 7.6×10^5 and for plate S2 of 7.8×10^5, which are in very good agreement.

CONCLUDING REMARKS

Six beryllium reflector plates have been used in the Plum Brook Reactor. All plates have bowed toward the fueled core with varying amounts of bow per unit dose. Two of these plates suffered structural failure and at different total doses. This behavior was evaluated in terms of plate materials and fabrication technique, preirradiation and postirradiation properties, the stresses experienced by the plates, and the mean power level of the reactor

The data available were not sufficient to permit firm conclusions to be drawn. However, the data available do indicate the following:

1. As fabricated mechanical property differences among the plates appeared to be negligible.

2. The internal stresses experienced by the irradiated plates probably approach the measured tensile strength of the material.

3. The amount of bow in the plates per unit dose is dependent on both the mean reactor power level and total dose at lower doses. At higher doses it is linearly proportional to the mean reactor power level alone.

4. The total dose to failure appears to be inversely proportional to the mean reactor power level.

Additional evaluations in progress will be reported when completed.

APPENDIX

NEUTRON SPECTRA AND DOSIMETRY

Dosimetry

The fast neutron fluence for the surveillance specimens was determined by using nickel dosimeter wires in the irradiation capsule. An effective cross section of 0.40 barns and a threshold of 2.9 Mev was used for the $Ni^{58}(n,P)Co^{58}$ reaction. The 0.1 Mev values were obtained by extrapolating the Ni data from 2.9 Mev using a spectral shape obtained by calculation. The calculated spectrum was a 71-group diffusion calculation. The thermal neutron fluence was monitored with cobalt wires using a cross section of 37.2 barns for the $Co^{59}(n,\gamma)Co^{60}$ reaction. The uncertainty (95 percent confidence) for the fast fluence is ±40 percent for $E_n > 0.1$ Mev. The uncertainty for the thermal fluence is ±10 percent.

The fast fluence for plate S1 was determined by analyzing samples of the plate after failure for iron and manganese-54. The specific activity resulting from the $Fe^{54}(n,p)Mn^{54}$ neutron was used to normalize the neutron spectrum for this location. The spectrum had been calculated using the SAND II code and experimentally determined activation data for several fast and intermediate flux detectors. The thermal fluences was estimated from 2 dimensional flux calculations for the PBR (Ref. 14). The uncertainties for both are estimated at ±40 percent at the 95 percent confidence level.

The fluences for plate S2 were determined by multiplying the fluences for plate S1 by the relative megawatt days of reactor exposure. There is some error introduced by this method for local fluence values of plate S2. Improved core loading has flattened the power distribution in the PBR core. Thus, the values shown in Table IV for plate S2 samples are somewhat high (~ 20 percent). The average fluence on the plate would not change.

Neutron Energy Spectra

The neutron energy spectra for the south beryllium plates at the reflector side are given in Figs. 9-11. The spectra for the surveillance specimens is similar but is complicated by the fact that they were irradiated in several different test facilities in the PBR.

REFERENCES

1. M. W. THOMPSON, Defects and Radiation Damage in Metals, Cambridge University Press (1969).

2. G. ROTH and V. NAUNDORF, "The Bulk Effect of Point Defects on Young's Modulus in Electron Irradiated Copper," Rad. Effects, 2, 141 (1970).

3. M. KANGIBASHI, "The Effects of Neutron Radiation on Structural Materials," REIC Report No. 45, Battelle Memorial Institute (1967).

4. W. FECYCH, "Experiences with Beryllium Swelling and Replacement In the Plum Brook Reactor, NASA TM X-52498 (1968).

5. L. I. MIRKIN, (J. E. S. Bradley, Trans.), Handbook of X-Ray Analysis of Polycrystalline Materials, Consultants Bureau (1964).

6. A. RUDNICK, C. W. MARSCHALL, W. H. DUCKWORTH, and B. R. EMRICH, "The Evaluation and Interpretation of Mechanical Properties of Brittle Materials," DCIC Report 68-3, Battelle Memorial Institute (1968).

7. R. SEDLACEK, "Tensile Strength of Brittle Materials," AFML-TR-65-129, Air Force Materials Luboratory (1965).

8. R. SEDLACEK, "Tensile Fatigue Strength of Brittle Materials," AFML-TR-66-245, Air Force Materials Laboratory (1968).

9. ANON., "Evaluation Test Methods For Beryllium," MAB-205-M, Materials Advisory Board, Division of Engineering, The National Academy of Sciences (1966).

10. G. E. KORTH and J. M. BEESTON, "Interim Report of Past-Irradiation Results of ATR Beryllium Surveillance Program," IN-1397, Idaho Nuclear Corp. (1970).

11. J. E. BOYD, Strength of Materials, Fifth ed., McGraw-Hill Book Co., Inc. (1950).

12. C. W. MARSCHALL and R. E. MARINGER, "Stress Relaxation as a Source of Dimensional Instability," J. Materials, 6, 374 (1971).

13. S. H. GELLES and A. RUDNICK, "Evaluation of Beryllium Foil Subjected to Biaxial Stresses," BMI-X-604, Battelle Memorial Institute (1970).

14. J. H. LYNCH, "Two Dimensional Flux and Criticality Calculations For the Plum Brook Reactor," NASA TN D-2210 (1964).

TABLE I

TYPICAL ANALYSIS OF BERYLLIUM FOR PLATES 2 AND 3

Composition

Element	Analysis
BeO	1.0 W/O
C	0.08
F_f	0.13
Al	0.07
Ni	0.01
Si	0.07
B	< 0.0002
Cd	< 0.0001
Li	0.0001
Co	< 0.0005
Mg	0.06

Mechanical Properties[a]

U.T.S. south plate 2	3.62×10^8 N/m^2(T); 2.9×10^8 N/m^2(L)
Y.S. (0.2 percent) south plate 2	2.5×10^8 N/m^2(T); 2.4×10^8 N/m^2(L)
Elongation south plate 2	4.3%(T); 1.1%(L)
U.T.S. south plate 3	2.8×10^8 N/m^2(T)
Y.S. south plate 3	1.9×10^8 N/m^2(T)
Elongation south plate 3	4.2%(T)

[a](T) = normal to pressing axis and for south plate 2, parallel to rolling direction.
(L) = parallel to pressing axis.

TABLE II

ENVIRONMENT

Parameter	Value	
	North plates	South plates
Cooling water temperature	338 K	338 K
Maximum plate temperature	< 390 K	390 K
Maximum fast neutron flux (E_n > 0.1 Mev)	1.2×10^{14} n/cm^2/sec	6.0×10^{14} n/cm^2/sec
Maximum thermal neutron flux	1.1×10^{15} n/cm^2/sec	1.0×10^{15} n/cm^2/sec

TABLE III

BOWING RATES FOR NORTH AND SOUTH PLATES

Plate[a]	Dose (D) (megawatt days)	Equivalent dose (D_e)[b] (megawatt days)	Bow (centimeters)	Bow/equivalent dose (B_d) (cm/MWD)	Failure dose (D_f) (MWD)
N1	25,256	5,060	0.052	1.02×10^{-5}	
N2	13,400	2,680	0.076	2.83×10^{-5}	
N3	2,437	487	0.0456	9.40×10^{-5}	
N3	14,946	3,000	0.104	3.47×10^{-5}	
S1	25,256	25,256	0.188	0.75×10^{-5}	37,256
S2	13,400	13,400	0.178	1.33×10^{-5}	23,223
S3	2,437	2,437	0.112	4.60×10^{-5}	
S3	14,946	14,946	0.254	1.69×10^{-5}	

[a] N1 = first north plate, etc.

[b] The fast flux on the north plate is 1/5 that on the south plate. The megawatt days are therefore multiplied by 1/5 for the north plates to obtain the true relative fluences on the north and south plates.

TABLE IV

ANALYSIS OF FAILED BERYLLIUM PLATES

Specimen number	Fast fluence >0.1 Mev, n/cm^2	Thermal fluence, n/cm^2	Density, $kg/m^3 \times 10^{-3}$	Lattice parameters A_o	Lattice parameters C_o	Gas content, cc/gm He	Gas content, cc/gm T_2	Dislocation loop density, no./cm^3
Plate number 1								
4Aa	4.2×10^{20}	1.7×10^{20}	$1.848 = 0.003$	2.2860 ± 0.00125	3.5844 ± 0.0001			6×10^{14}
4Ab	4.2×10^{20}	1.7×10^{20}	1.848	2.2865	3.5842			
11a	4.2×10^{21}	1.0×10^{22}		2.2865	3.5848			
11b	4.2×10^{21}	1.0×10^{22}		2.2860	3.5851			
12c	3.9×10^{21}	9.0×10^{21}		2.2860	3.5848			
16E	1.4×10^{22}	2.4×10^{22}		2.2870	3.5867	6.85	0.335	1×10^{15}
16F	1.4×10^{22}	2.4×10^{22}		2.2870	3.5867	5.64	0.292	
20Ba	2.1×10^{22}	4.3×10^{22}	1.836					5×10^{15}
22Aa-1	2.4×10^{22}	4.9×10^{22}				12.56	0.25	
22Aa-2	↓	↓				10.35	0.60	
22Ba			1.832			10.08	0.91	
22Bb			1.838					
22A				2.2875	3.5875			
22CC						10.25	0.483	
23a	1.3×10^{22}	4.7×10^{22}	1.820			6.22	0.52	
23b	1.3×10^{22}	4.7×10^{22}	1.832					

TABLE IV

CONTINUED

Specimen number	Fast fluence >0.1 Mev, n/cm^2	Thermal fluence, n/cm^2	Density, $kg/m^3 \times 10^{-3}$	Lattice parameters A_o	Lattice parameters C_o	Gas content, cc/gm He	Gas content, cc/gm T_2	Dislocation loop density, $no./cm^3$
Plate number 2								
10Aa	5.2×10^{20}	2.1×10^{20}	1.853	2.2858	3.5845			9×10^{14}
10Ab	5.2×10^{20}	2.1×10^{20}		2.2862	3.5842			
37A	5.9×10^{21}	1.0×10^{22}		2.2865	3.5850			
43A	1.1×10^{22}	2.2×10^{22}	1.852					
45A	1.5×10^{22}	3.0×10^{22}	1.949	2.2865	3.5848	4.04	0.31	
45Ba	↓	↓				4.17	0.31	
45Bb						4.22	0.31	
45C			1.851			3.48	0.26	
45D						6.14	0.05	6×10^{15}
47A	6.1×10^{21}	1.2×10^{22}						1×10^{15}

TABLE V

BERYLLIUM SURVEILLANCE SPECIMEN DATA

Test number	Fast fluence, >0.1 Mev n/cm^2	Thermal fluence, n/cm^2	Density change, kg/m^3	Ultimate tensile strength, $(N/m^2)x10^{-8}$		Bend strength load at fracture- $Nx10^{-2}$		Hardness Rockwell B	
				Pre	Post	Pre	Post	Pre	Post
Plate S1									
2	$9.3x10^{20}$	$1.8x10^{21}$	----	2.9±0.2	2.4-2.9	2.1±0.1	2.7-2.9	77	80
3	$1.3x10^{21}$	$2.5x10^{21}$	----	↓	3.7-3.8	↓	2.5-2.8	74	93
4	$4.1x10^{21}$	$9.2x10^{21}$	----		1.5-2.8		2.1-2.6	76	87
5	$4.8x10^{21}$	$9.6x10^{21}$	-1±3		4.2-4.4		1.5-1.8	75	94
x	$9.2x10^{21}$	$1.7x10^{22}$	-9±3		1.2-1.7		2.3-3.2	75	97
Plate S2									
1	$8.6x10^{20}$	$2.9x10^{21}$	----	3.08±0.2	2.8-4.2	2.4±0.1	-------	71	79
2	$1.7x10^{21}$	$5.8x10^{21}$	----	All test 2 tensile specimens failed in grips		-------	-------	70	97

TABLE VI

EVALUATION OF BOWING CONSTANTS[a]

Plate	Equivalent dose (MWD)	B_d (cm/MWD)	$\overline{P}_r$ (megawatts)	K_B
N1	5,060	1.02×10^{-5}	18.1	5.6×10^{-7}
N2	2,680	2.83×10^{-5}	31.1	9.1×10^{-7}
N3	487	9.40×10^{-5}	49.7	19×10^{-7}
N3	3,000	3.47×10^{-5}	42.1	8.3×10^{-7}
S1	25,256	7.45×10^{-5}	18.1	4.1×10^{-7}
S2	13,400	1.33×10^{-5}	31.1	4.3×10^{-7}
S3	2,437	4.60×10^{-5}	49.7	9.3×10^{-7}
S3	14,946	1.69×10^{-5}	42.1	4.0×10^{-7}

[a] $K_B = \frac{B_D}{\overline{P}_r}$

E-6499

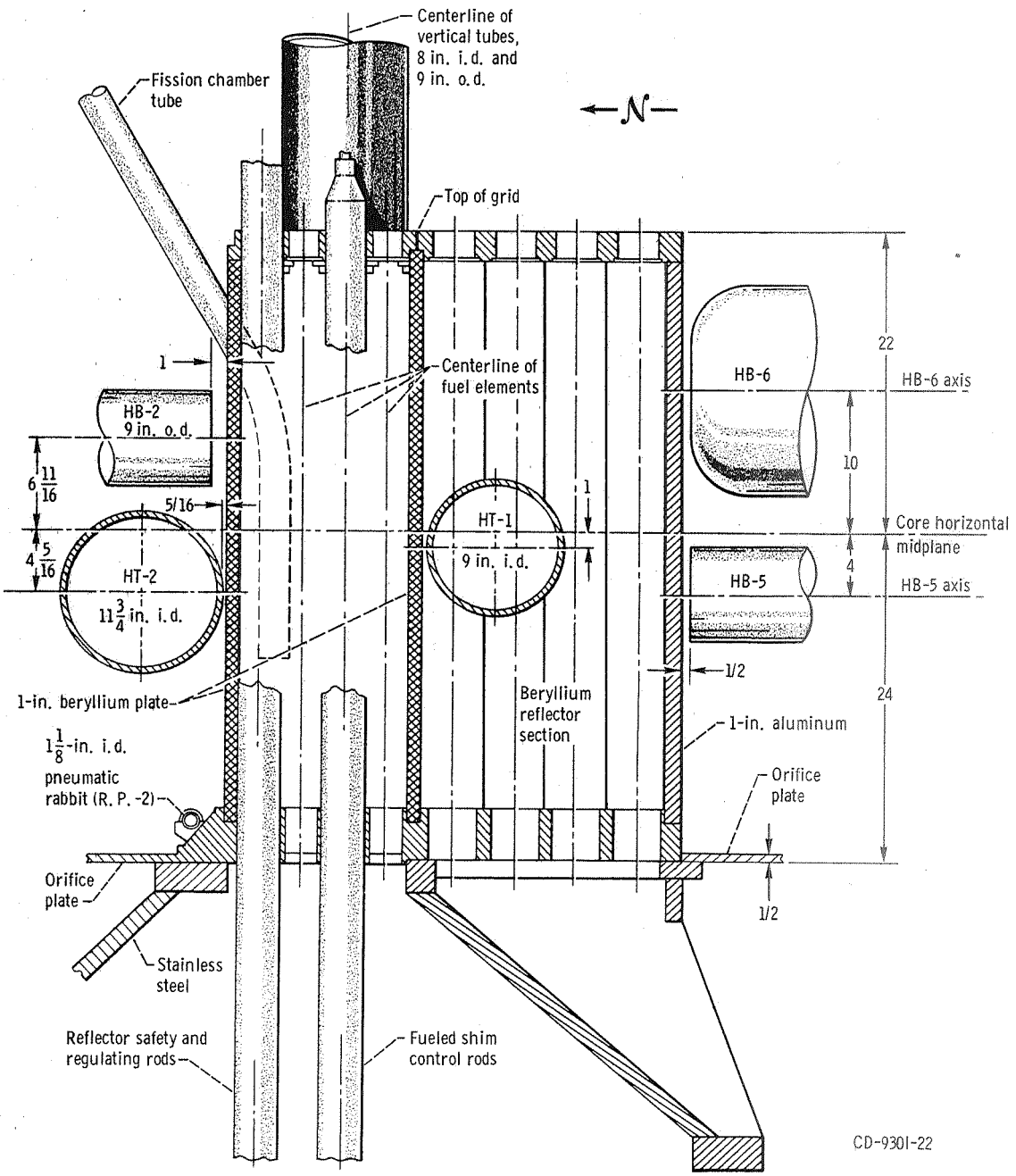

Figure 1. - Reactor Core - Vertical Section

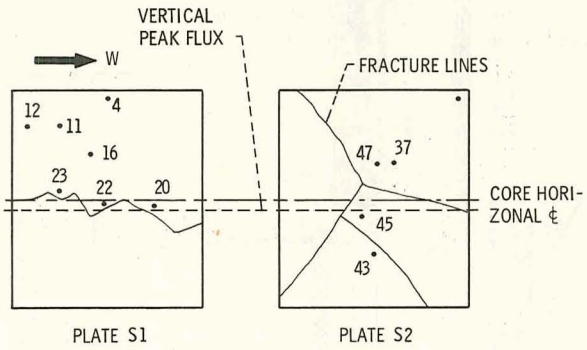

Figure 2. - Plate sample and fracture locations.

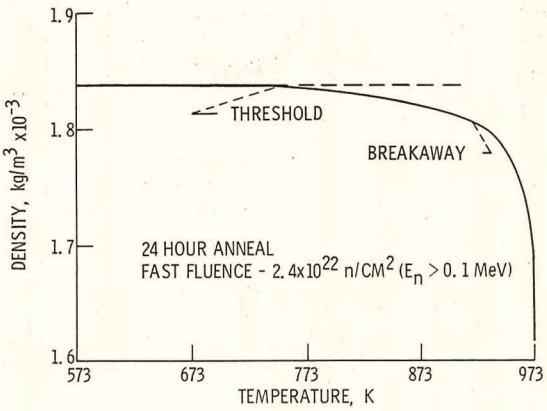

Figure 3. - Swelling threshold plate number S1 beryllium.

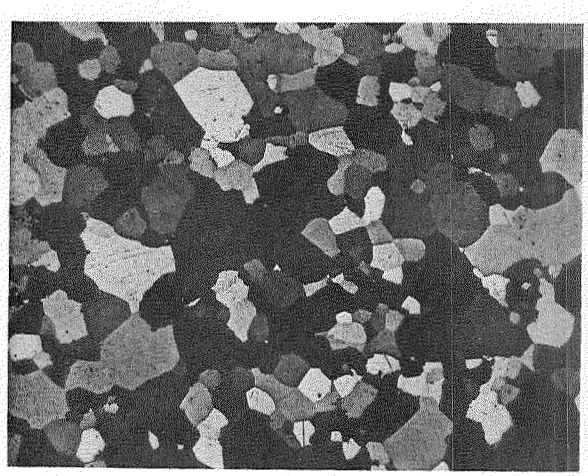

(A) PLATE S1.

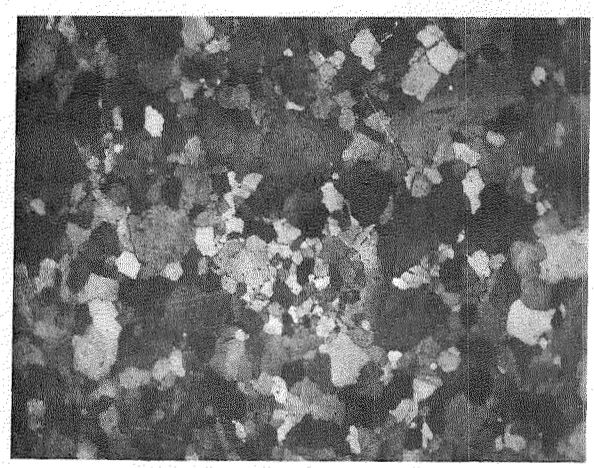

(B) PLATE S2.

Figure 4. - Microstructure of plates S1 and S2. X250.

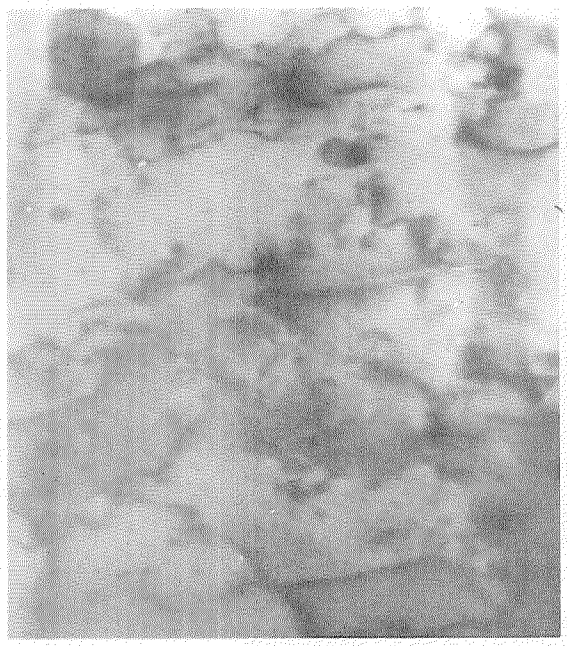

(A) 4Da LOW FLUX REGION.

(B) 16Ca INTERMEDIATE FLUX REGION.

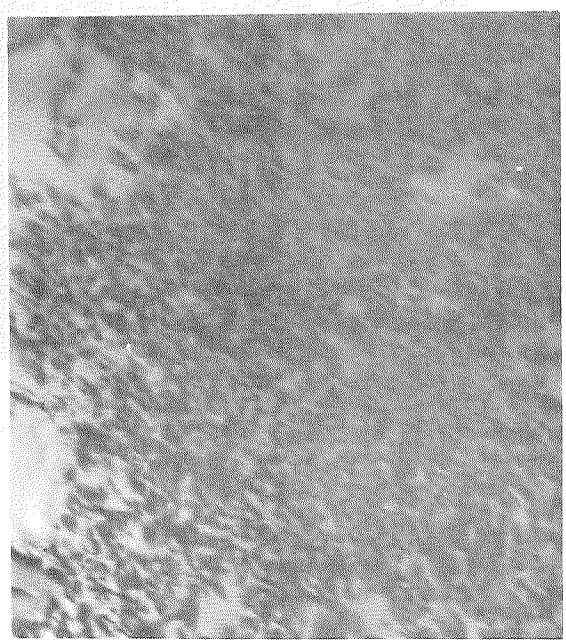

0.2 μ

(C) 20Ba HIGH FLUX REGION.

Figure 5. - Transmission electron micrographs of samples taken from various regions of moderator plate 1.

(A) 10a REGION OF LOW FLUX.

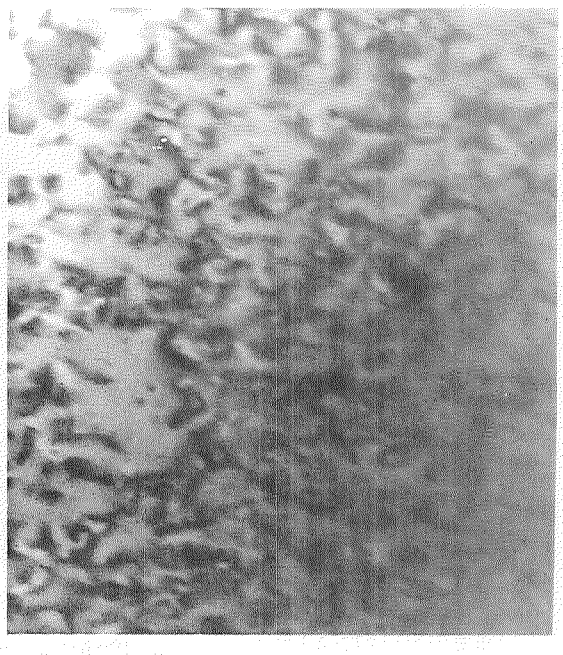

(B) 47a REGION OF INTERMEDIATE FLUX.

0.2 μ

(C) 45d REGION OF HIGH FLUX.

Figure 6. - Transmission electron micrographs of samples taken from various regions of moderator plate 2.

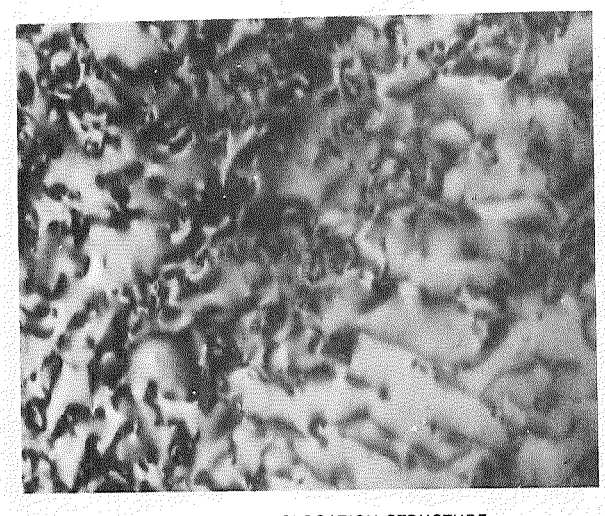

(A) GENERAL DISLOCATION STRUCTURE.

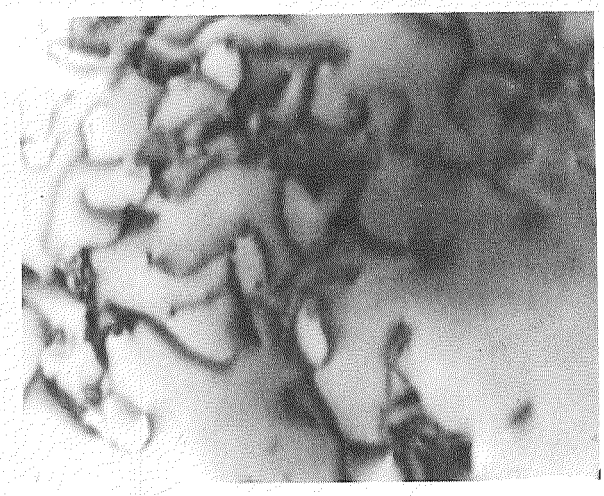

0.1 μ (B) DISLOCATION INTERACTIONS.

Figure 7. - Dislocation structure of sample 20B from plate S1.

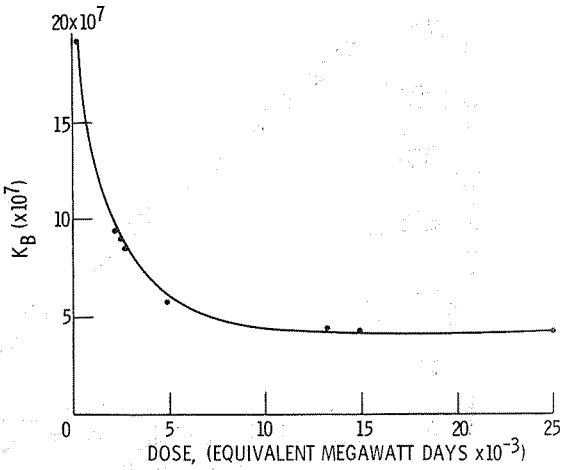

Figure 8. - Bowing constant as a function of equivalent dose.

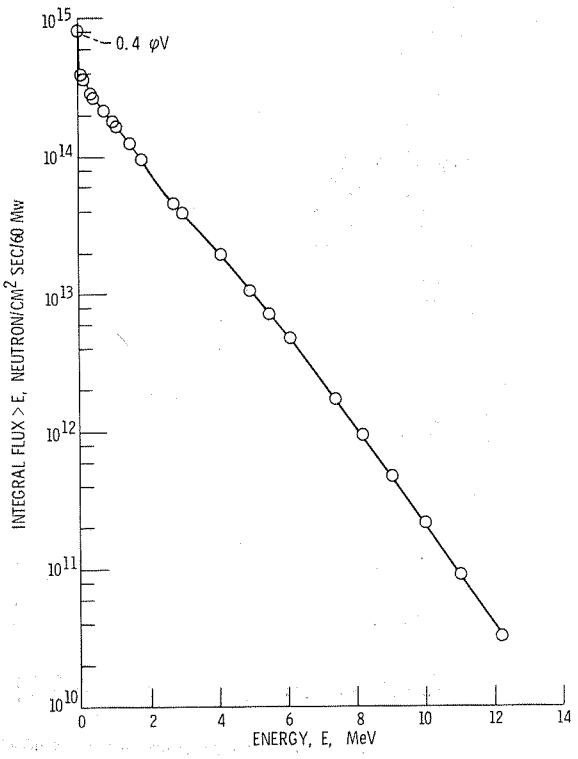

Figure 9. - Integral neutron spectrum south Be plate.

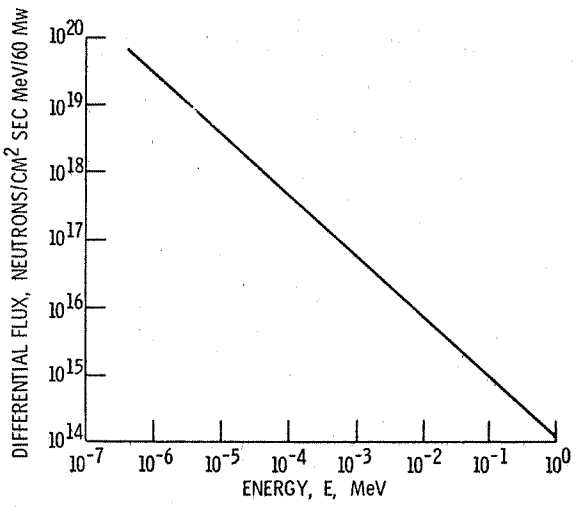

Figure 10. - Differential neutron spectrum south Be plate.

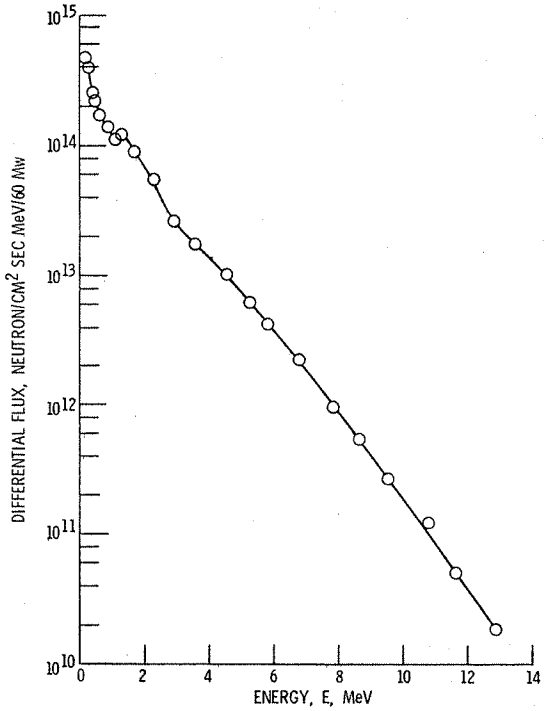

Figure 11. - Differential neutron spectrum south Be plate.